

# First Demonstration of MeV-Scale Physics in Liquid Argon Time Projection Chambers Using ArgoNeuT

R. Acciarri,<sup>1</sup> C. Adams,<sup>2</sup> J. Asaadi,<sup>3</sup> B. Baller,<sup>1</sup> T. Bolton,<sup>4</sup> C. Bromberg,<sup>5</sup> F. Cavanna,<sup>1</sup> E. Church,<sup>6</sup>  
D. Edmunds,<sup>5</sup> A. Ereditato,<sup>7</sup> S. Farooq,<sup>4</sup> A. Ferrari,<sup>8</sup> R.S. Fitzpatrick,<sup>9</sup> B. Fleming,<sup>2</sup> A. Hackenburg,<sup>2</sup>  
G. Horton-Smith,<sup>4</sup> C. James,<sup>1</sup> K. Lang,<sup>10</sup> M. Lantz,<sup>11</sup> I. Lepetic,<sup>12,\*</sup> B.R. Littlejohn,<sup>12,†</sup> X. Luo,<sup>2</sup>  
R. Mehdiyev,<sup>10</sup> B. Page,<sup>5</sup> O. Palamara,<sup>1</sup> B. Rebel,<sup>1</sup> P.R. Sala,<sup>13</sup> G. Scanavini,<sup>2</sup> A. Schukraft,<sup>1</sup>  
G. Smirnov,<sup>8</sup> M. Soderberg,<sup>14</sup> J. Spitz,<sup>9</sup> A.M. Szelc,<sup>15</sup> M. Weber,<sup>7</sup> W. Wu,<sup>1</sup> T. Yang,<sup>1</sup> and G.P. Zeller<sup>1</sup>

(The ArgoNeuT Collaboration)

<sup>1</sup>*Fermi National Accelerator Lab, Batavia, Illinois 60510, USA*

<sup>2</sup>*Yale University, New Haven, Connecticut 06520, USA*

<sup>3</sup>*University of Texas at Arlington, Arlington, Texas 76019, USA*

<sup>4</sup>*Kansas State University, Manhattan, Kansas 66506, USA*

<sup>5</sup>*Michigan State University, East Lansing, Michigan 48824, USA*

<sup>6</sup>*Pacific Northwest National Lab, Richland, Washington 99354, USA*

<sup>7</sup>*University of Bern, 3012 Bern, Switzerland*

<sup>8</sup>*CERN, CH-1211 Geneva 23, Switzerland*

<sup>9</sup>*University of Michigan, Ann Arbor, Michigan 48109, USA*

<sup>10</sup>*University of Texas at Austin, Austin, Texas 78712, USA*

<sup>11</sup>*Uppsala University, 751 20 Uppsala, Sweden*

<sup>12</sup>*Illinois Institute of Technology, Chicago, Illinois 60616, USA*

<sup>13</sup>*INFN Milano, INFN Sezione di Milano, I-20133 Milano, Italy*

<sup>14</sup>*Syracuse University, Syracuse, New York 13244, USA*

<sup>15</sup>*University of Manchester, Manchester M13 9PL, United Kingdom*

MeV-scale energy depositions by low-energy photons produced in neutrino-argon interactions have been successfully identified and reconstructed in ArgoNeuT liquid argon time projection chamber (LArTPC) data. ArgoNeuT data collected on the NuMI beam at Fermilab were analyzed to identify isolated low-energy depositions in the TPC volume. The total number, reconstructed energies and positions of these depositions have been compared to those from simulations of neutrino-argon interactions using the FLUKA Monte Carlo generator. Measured features are consistent with energy depositions from photons produced by de-excitation of the neutrino's target nucleus and by inelastic scattering of primary neutrons produced by neutrino-argon interactions. This study represents the first successful reconstruction of physics at the MeV-scale in a LArTPC, a capability of crucial importance for detection and reconstruction of supernova and solar neutrino interactions in future large LArTPCs.

## I. INTRODUCTION

The Liquid Argon Time Projection Chamber (LArTPC) is a powerful detection technology for neutrino experiments, as it allows for millimeter spatial resolution, provides excellent calorimetric information for particle identification, and can be scaled to large, fully active, detector volumes. LArTPCs have been used to measure neutrino-argon interaction cross sections and final-state particle production rates in the case of ArgoNeuT [1–7] and MicroBooNE [8], neutrino oscillations in the case of ICARUS [9], and charged particle interaction mechanisms on argon in the case of LArIAT [10].

LArTPCs are being employed to make important measurements, e.g. understanding the neutrino-induced low-energy excess of electromagnetic events with Micro-

BooNE [11] and will be used to search for sterile neutrinos in the Fermilab SBN program [12] and for CP-violation in the leptonic sector with DUNE [13]. Precise measurements of neutrino-argon cross sections will be performed with SBN [12] and of charged hadron interactions with ProtoDUNE [14]. In most of the existing measurements, LArTPCs were placed in high energy neutrino beams to study GeV-scale muon and electron neutrinos as well as final-state products, generally with energies greater than 100 MeV. A smaller number of measurements have investigated particles or energy depositions in the  $\sim 10 - 100$  MeV range [6, 15, 16], some using scintillation light [17].

No existing measurements have demonstrated LArTPC capabilities at the MeV scale for neutrino experiments, despite the wealth of physics studies that have been proposed for future large LArTPCs in this energy range. A number of studies have investigated expected supernova and solar neutrino interaction rates in the DUNE experiment: see Refs. [13] and [18] for reviews and relevant citations. Other studies have

\* ilepetic@hawk.iit.edu

† blittlej@iit.edu

61 proposed using decay-at-rest neutrino interactions  
 62 for short-baseline oscillation tests, coherent neutrino  
 63 scattering measurements and supernova-related stud-  
 64 ies [19–23]. LArTPC experiments utilizing GeV-scale  
 65 neutrino beamlines would also benefit from the ability  
 66 to perform a reconstruction of MeV-scale features. This  
 67 ability would allow for a fuller reconstruction of beam  
 68 neutrino events by enabling reconstruction of photons  
 69 released during de-excitation of the nucleus and of part  
 70 of the energy transferred to final-state neutrons. Fur-  
 71 thermore, MicroBooNE has shown that identifying and  
 72 including full reconstructed energies at ends of showers  
 73 is challenging and would benefit from the ability to  
 74 reconstruct Compton scatters of photons exiting the  
 75 shower core [15].

76 Performing identification and reconstruction of parti-  
 77 cles at MeV energies in a LArTPC is a challenging and  
 78 previously unattempted task. At higher energies ( $> 100$   
 79 MeV), charged particles travel several centimeters to me-  
 80 ters in distance, leaving detectable signals on dozens to  
 81 hundreds of TPC wires, producing an ionization track  
 82 that can be utilized for reconstructing the identity and  
 83 kinematics of detected particles. On the other hand,  
 84 charged particles with kinetic energies near the MeV  
 85 scale travel a distance of the order of or less than the  
 86 distance between adjacent wires in many LArTPCs (3-  
 87 5 mm), leaving just one hit or a short cluster of a few  
 88 consecutive hits. Thus, current analysis methods used to  
 89 reconstruct physics quantities from tracks made of large  
 90 numbers of wire signals are ineffective in this energy  
 91 regime, and there is a need for new, low-energy-specific  
 92 methods.

93 We have used data acquired by the ArgoNeuT  
 94 LArTPC detector at Fermilab to search for small energy  
 95 depositions associated with neutrino events and com-  
 96 pared them to predictions from the FLUKA neutrino in-  
 97 teraction generator [24–26]. Using new topological re-  
 98 construction tools, we find clear evidence of activity due  
 99 to de-excitation of the final-state nucleus and inelastic  
 100 scattering of neutrons in the detector.

101 We begin with a description of the ArgoNeuT detec-  
 102 tor in Section II. We then overview nuclear de-excitation  
 103 photon production, photon emission from inelastic scat-  
 104 tering of neutrons, and photon propagation in argon in  
 105 Section III. We then describe utilized datasets and recon-  
 106 struction in Sections IV and V. Final reconstructed sig-  
 107 nal distributions are presented and compared to a Monte  
 108 Carlo (MC) simulation in Section VI.

## 109 II. THE ARGONEUT DETECTOR

110 ArgoNeuT was a LArTPC experiment which was  
 111 placed in the Neutrinos at the Main Injector (NuMI)  
 112 beamline at Fermilab for five months in 2009-2010. Ar-  
 113 goNeuT was located 100 m underground, in front of

114 the MINOS near detector (MINOS ND). The TPC was  
 115  $47(w) \times 40(h) \times 90(l)$  cm<sup>3</sup> with a volume of 169 L.  
 116 Ionized charge drifted in the x-direction by means of an  
 117 electric field produced by a cathode biased at a negative  
 118 high voltage of magnitude 23.5 kV. A field shaping cage  
 119 caused the electric field along the drift length to be uni-  
 120 form at 481 V/cm. The resulting drift velocity was 1.57  
 121 mm/ $\mu$ s, with a maximum drift time of 300.5  $\mu$ s. At the  
 122 anode end of the TPC there were three wire planes, of  
 123 which two were instrumented (the innermost plane was  
 124 a shield plane). The middle wire plane was the induc-  
 125 tion plane; the outer one was the collection plane. Each  
 126 of the instrumented planes was comprised of 240 wires,  
 127 with a wire spacing of 4 mm and oriented at  $\pm 60^\circ$  to  
 128 the z-axis (beam direction). In each detector readout,  
 129 each wire channel was sampled every 198 ns, for a total  
 130 readout window of 405  $\mu$ s. The waveform for each  
 131 wire was recorded with hits identified from peaks above  
 132 baseline. Triggering for a readout was determined by the  
 133 NuMI beam spill, at a rate of 0.5 Hz. A more detailed  
 134 description and operational parameters of the ArgoNeuT  
 135 detector are given in [27].

136 ArgoNeuT benefited from the presence of the MINOS  
 137 ND located immediately downstream of it. The MI-  
 138 NOS ND is a segmented magnetized steel and scintil-  
 139 lator detector [28]. As a result, the momenta and signs of  
 140 muons which were produced by neutrino interactions in  
 141 ArgoNeuT and entered the MINOS ND could be deter-  
 142 mined by using information from the MINOS ND. Ar-  
 143 goNeuT also benefited from its placement 100 m under-  
 144 ground; at this depth, cosmic rays are expected to be seen  
 145 in fewer than 1 in 7000 triggers.

146 During the majority of ArgoNeuT’s run, the NuMI  
 147 beam was operated in the low energy antineutrino mode;  
 148 neutrino fluxes produced during this operation mode are  
 149 described in [2]. The composition of the beam was 58%  
 150 muon neutrino, 40% muon antineutrino, and 2% elec-  
 151 tron neutrino and antineutrino. The average energy for  
 152 muon neutrinos was 9.6 GeV, and the average energy of  
 153 muon antineutrinos was 3.6 GeV. The antineutrino mode  
 154 run lasted 4.5 months with  $1.25 \times 10^{20}$  protons on target  
 155 (POT) acquired.

## 156 III. PRODUCTION AND INTERACTION OF 157 LOW-ENERGY PHOTONS IN NEUTRINO-ARGON 158 INTERACTIONS

159 MeV-energy photons can be produced in neutrino-  
 160 argon interactions by two possible mechanisms, de-  
 161 excitation of the target nucleus and inelastic scattering  
 162 of final-state particles. When a neutrino interacts with an  
 163 <sup>40</sup>Ar nucleus, the target nucleon and the neutrino inter-  
 164 action products initiate a nuclear reaction during which  
 165 nucleons and nuclear fragments may be emitted. The re-  
 166 maining residual nucleus is often left in an excited state.

167 The nucleus de-excites by means of the emission of a  
 168 photon or cascade of photons with energies ranging from  
 169  $\sim 0.1$  MeV – 10 MeV. Reaction products heavier than  
 170 deuterons and the recoiling residual nucleus are gener-  
 171 ally not observable in a LArTPC. Final-state neutrons  
 172 which inelastically scatter off an  $^{40}\text{Ar}$  nucleus or are cap-  
 173 tured by it will also produce photons in the energy range  
 174 of interest as the  $^{40}\text{Ar}$  nucleus de-excites [29].

175 As photons are neutral particles, they cannot be de-  
 176 tected directly. Instead we detect electrons resulting from  
 177 a photon interaction. The scale of the distance between  
 178 subsequent energy depositions for one photon is given  
 179 by the radiation length ( $X_0$ ), which in liquid argon is 14  
 180 cm. Over the  $\sim 0.1 - 10$  MeV range of interest in this  
 181 study, the most probable interaction process for photons  
 182 in LAr is Compton scattering. In Compton scattering at  
 183 this energy, each photon has a high probability of cre-  
 184 ating multiple topologically isolated energy depositions  
 185 within a LArTPC. Higher energy photons can also inter-  
 186 act via pair-production, however this is still subdominant  
 187 in the energy range considered here.

#### 188 A. Neutrino interactions and neutron scattering in 189 FLUKA

190 The only neutrino MC interaction generator that in-  
 191 cludes the simulation of both mechanisms of low-energy  
 192 photon production in GeV-scale neutrino interactions in  
 193 argon is FLUKA [24–26]. FLUKA is a multi-particle  
 194 transport and interaction code. Its neutrino interaction  
 195 generator, called NUNDIS[26], is embedded in the same  
 196 nuclear reaction module of FLUKA used for all hadron-  
 197 induced reactions. Quasi elastic, resonant ( $\Delta$  produc-  
 198 tion only) and deep inelastic scattering interactions are  
 199 modeled on single nucleons according to standard for-  
 200 malisms. Initial state effects are accounted for by con-  
 201 sidering bound nucleons distributed according to a Fermi  
 202 momentum distribution. Final-state effects include a  
 203 generalized intranuclear cascade (G-INC), followed by a  
 204 pre-equilibrium stage and an evaporation stage. As men-  
 205 tioned above, nucleons, mesons and nuclear fragments  
 206 can be emitted during these stages. Residual excitation is  
 207 dissipated through photon emission. Experimental data  
 208 on nuclear levels and photon transitions are taken into  
 209 account whenever available.

210 Neutron-induced reactions are treated as standard  
 211 hadronic interactions for neutron energies above 20 MeV,  
 212 while for energies below 20 MeV a data-driven treat-  
 213 ment is used, as in most low-energy neutron transport  
 214 codes. Reaction cross sections, branching ratios and  
 215 emitted particle spectra are imported from publicly avail-  
 216 able databases. Transport is based on a multi-group ap-  
 217 proach (neutron energies grouped in intervals, cross sec-  
 218 tions averaged within groups), except for selected reac-  
 219 tions [24]. In the FLUKA version used for this work

220 (FLUKA2017, not yet released), a special treatment has  
 221 been implemented for reactions on  $^{40}\text{Ar}$ . Cross sections  
 222 are evaluated point-wise (for the exact neutron energy),  
 223 correlations among reaction products are included, and  
 224 gamma de-excitation is simulated as a photon cascade  
 225 following experimental energies and branching ratios.

226 Figure 1 shows the energies and numbers of pho-  
 227 tons from charged current interactions of muon neutrinos  
 228 from the NuMI beam interacting and depositing energy  
 229 in a volume of liquid argon with the dimensions of Ar-  
 230 goNeuT, according to FLUKA simulation (see Section  
 231 IV for details). A significant overlap in both the en-  
 232 ergies and numbers of photons from the two processes  
 233 (de-excitation of the target nucleus and inelastic neutron  
 234 scattering) is visible, making separation of the source of  
 235 energy depositions difficult based on these metrics alone.  
 236 Considering ArgoNeuT’s size, a photon could leave the  
 237 TPC with a significant amount of its energy undetected.  
 238 It is also notable that 24% of product nuclei in this simu-  
 239 lation are found in the ground state and produce no pho-  
 240 tons.

241 Typically, low energy photon-produced electrons are  
 242 expected to appear in a LArTPC event display as blips  
 243 from isolated energy depositions around the neutrino in-  
 244 teraction vertex. An example can be seen in Fig. 2,  
 245 where a typical ArgoNeuT neutrino event is shown.

## 246 IV. DATASETS

247 This analysis uses two primary real datasets from the  
 248 antineutrino mode run. Events with simple, low track  
 249 multiplicity final-state topology have been selected for  
 250 the present analysis, as more complex events make the  
 251 selection of isolated low-energy signatures more diffi-  
 252 cult. The first dataset, termed the neutrino dataset, is  
 253 a subsample of muon neutrino and antineutrino events  
 254 from the ArgoNeuT charged current pion-less (CC  $0\pi$ )  
 255 events sample, i.e. muon (anti)neutrino charged current  
 256 events that do not produce pions in the final state. This  
 257 sample of events with simple topologies was chosen in  
 258 order to more easily identify low energy gamma activ-  
 259 ity. The selection and analysis of these events [5], re-  
 260 quires that a three dimensional (3D) track reconstructed  
 261 in the LArTPC is matched to a MINOS ND muon track,  
 262 and that any number of tracks at the vertex, identified as  
 263 protons using the algorithm defined in [27], are present  
 264 in the final state ( $\mu + Np$  events). In addition, we re-  
 265 quire that none of the events contains a reconstructed  
 266 3D track identified as a charged pion or a reconstructed  
 267 shower corresponding to an electron or high-energy pho-  
 268 ton. The threshold for proton (pion) identification is 21  
 269 (10) MeV [3]. From the CC  $0\pi$ -pion sample we have se-  
 270 lected a subsample of events with one muon and up to  
 271 one proton in the final state (CC  $0\pi$ , 0 or 1 proton events)  
 272 for the present analysis. The second dataset, termed the

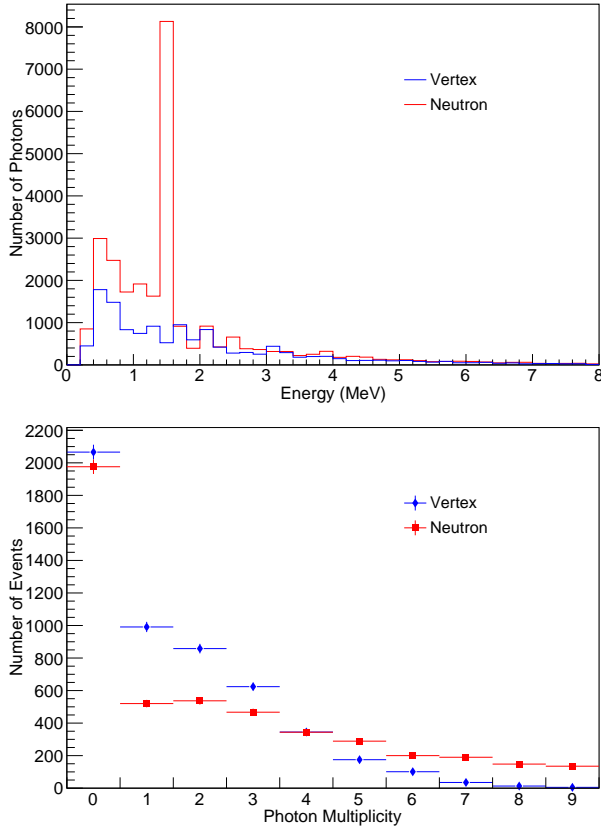


FIG. 1. Energy (top) and multiplicity (bottom) of low-energy photons from charged current interactions of muon neutrinos from the NuMI beam interacting and depositing energy in a volume of liquid argon with the dimensions of ArgoNeuT. Color indicates source of photon (blue are de-excitation photons, red are photons produced by neutrons). For a photon to be tracked in the simulation, it must have an energy  $\geq 0.2$  MeV. The peak at 1.46 MeV corresponds to the first excited state of  $^{40}\text{Ar}$ .

background dataset, was obtained by examining “empty event” triggers which do not appear to contain a neutrino interaction but do contain ambient gamma ray backgrounds, intrinsic  $^{39}\text{Ar}$  activity, and electronics noise. The beta emitter  $^{39}\text{Ar}$  is a radioactive isotope found in natural argon; at a rate of  $10^{-5}$  Bq/L, it is not expected to be a large background in ArgoNeuT events. Electronics noise can be identified as a hit if the deviation from the baseline is above a threshold. These features are also present in the neutrino events previously described, so the background dataset is used for a data-driven modeling of the background in the selected neutrino events.

ArgoNeuT data are compared with a MC dataset, generated using the FLUKA MC neutrino interaction generator. We produced simulated neutrino interactions in ArgoNeuT using FLUKA and the energy spectrum of the NuMI beamline. A simplified ArgoNeuT detector geometry was inserted into FLUKA. In addition to produc-

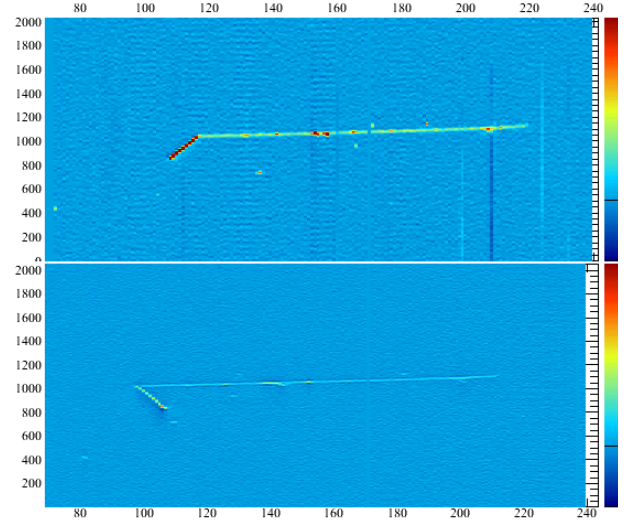


FIG. 2. A neutrino event (raw data) with one (longer) track reconstructed as a muon exiting the detector and one (shorter) track reconstructed as a proton. Possible photon activity (isolated blips) is visible in the event (e.g. collection plane wire 135, time 700). The top image is the collection plane, and the bottom image is the induction plane. Wire number is indicated on the horizontal axis. The vertical axis indicates sample number. Color indicates amount of charge collected.

ing all the final-state particles emerging from the neutrino interaction, including hadron re-interaction inside the nucleus (nuclear effects), FLUKA also simulates the physics of the final-state nucleus, resulting in the production of final-state de-excitation photons. FLUKA was also used to propagate final-state neutrons inside the LAr volume, resulting in the simulation of energies and locations of secondary neutron-produced photons. The FLUKA-determined properties of non-neutron final-state particles and secondary neutron-produced photons were then used as input to a LArSoft [30] MC simulation of ArgoNeuT and propagated through the detector simulation, signal processing, and reconstruction stages as for real data. CC  $0\pi 0$ , 1 proton events, i.e. events with one muon track entering the MINOS ND and up to one additional proton with kinetic energy  $> 21$  MeV and no pions with kinetic energy  $> 10$  MeV in the final state, compose the selected MC samples for the present analysis. Electronics noise, and ambient and internal radioactivity were not simulated; the background dataset described above was instead used to directly include these contributions to the MC dataset.

## V. EVENT RECONSTRUCTION

As discussed in Section III, the radiation length in liquid argon is 14 cm, and MeV photon-produced electrons

316 have ranges of a millimeter to a centimeter, as shown in  
 317 Fig. 3. Consequently, for the present analysis a signal  
 318 on the wire planes consists of a single hit or a very short  
 319 cluster of hits on consecutive wires on both active planes  
 320 of the TPC, topologically isolated from the rest of the  
 321 event's features, possibly concentrated around the inter-  
 322 action vertex, as shown in Fig. 2.

323 The same reconstruction procedure has been applied  
 324 to all the selected data and MC samples described in the  
 325 previous Section. The reconstruction proceeded through  
 326 two steps, one “standard” reconstruction step based on  
 327 LArSoft, followed by a low-energy specific second step,  
 328 described in Section V A.

329 First, the “standard” ArgoNeuT automated reconstruc-  
 330 tion procedure, including hit finding, hit reconstruction  
 331 and track reconstruction, as described in detail in [7],  
 332 was applied. Events were required to have a recon-  
 333 structed neutrino interaction vertex contained in the fidu-  
 334 cial detector volume, defined as [3, 44] cm along the drift  
 335 direction, [-16, 16] cm vertically from the center of the  
 336 detector, and [6, 86] cm along the beam. The neutrino  
 337 and background datasets contain 552 and 1970 events,  
 338 respectively.

### 339 A. Signal Selection

340 In the second step, a low-energy specific procedure to  
 341 identify and reconstruct isolated hits and clusters was  
 342 applied. Since low-energy electrons will leave short  
 343 isolated features in the TPC, hits that are identified as  
 344 belonging to a reconstructed track longer than 1.5 cm  
 345 and beginning at the neutrino interaction vertex were re-  
 346 moved. To also remove nearby wire activity associated  
 347 with a track (such as delta rays), all hits inside a  $120^\circ$   
 348 cone around the first 2.4 cm of each reconstructed track  
 349 and a 5 cm cylinder along the remaining track length  
 350 were rejected. For tracks reconstructed as being longer  
 351 than 4 cm, the cylindrical rejection region was extended  
 352 past the end of the track, in case the automated recon-  
 353 struction cuts the track short. Then, several cuts were  
 354 made on the remaining hits found in each event. A  
 355 threshold cut removed hits whose fitted peak height is  
 356 below a certain ADC count threshold on the induction  
 357 and collection planes (6 and 10 ADC, respectively), cor-  
 358 responding to roughly 0.2 MeV of energy deposited. Hits  
 359 whose fitted peak height is above a maximum ADC count  
 360 (60 ADC, corresponding to  $\sim 1.2$  MeV) were also re-  
 361 moved, as they were unlikely to be produced by photon  
 362 energy depositions. As shown in Fig. 3, such hits are  
 363 more likely due to protons. For example, for a proton  
 364 to travel a distance of 0.4 cm, the wire spacing, it must  
 365 have a kinetic energy of at least 21 MeV, well above the  
 366 maximum ADC cut. On the other hand, an electron must  
 367 have a kinetic energy of 1 MeV to travel the same dis-  
 368 tance. Low energy protons with very short range can re-

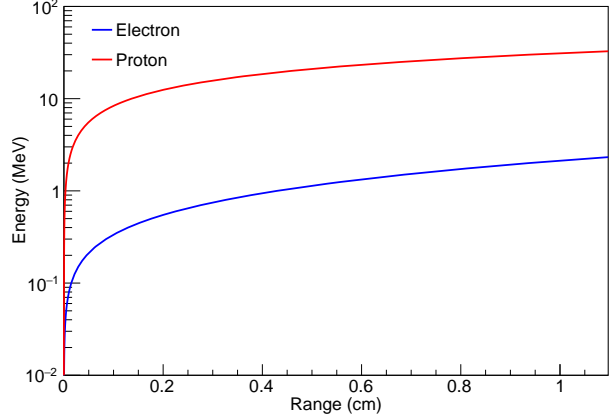


FIG. 3. Energy vs range for electrons and protons for the ranges of interest for this study. Red denotes protons, blue denotes electrons. The clear separation between electron and proton means it is unlikely a proton hit will be mistakenly identified as an electron hit. Data from [31].

369 sult from a neutron-proton reaction on argon, however  
 370 the FLUKA simulation indicates fewer than 1% of hits  
 371 passing cuts are due to protons. A fiducial cut was then  
 372 applied to remove all hits within 6 cm of the cathode and  
 373 anode and hits near corners of the TPC.

374 To suppress hits originating from above-threshold  
 375 electronics noise, matching of hit times between induc-  
 376 tion and collection planes was required. This plane  
 377 matching also allowed for reconstruction of the 3D space  
 378 position for all hits in the final sample passing the above  
 379 selection criteria. Applied cuts are visually demonstrated  
 380 in Fig. 4.

381 After the selection was complete, events were individ-  
 382 ually visually scanned to remove noisy wires and recon-  
 383 struction failures. Individual wires were removed on an  
 384 event by event basis if it was clear they had several hits  
 385 due to electronics noise, with equivalent cuts applied to  
 386 nearby background events. Some hits were also manu-  
 387 ally removed if it was clear they belonged to a track that  
 388 was not reconstructed properly.

389 A summary of the level of hit removal achieved in each  
 390 cut for neutrino, background and MC datasets is found  
 391 in Table I. Once all cuts were applied and handscan-  
 392 ning was complete, the resulting neutrino (background)  
 393 datasets contained 716 (422) collection plane selected  
 394 hits in 552 (1970) events.

395 Following this selection, we grouped signal hits into  
 396 clusters and attempted a reconstruction of clusters' po-  
 397 sitions and energies. A cluster is defined as a collection of  
 398 one or more signals on adjacent wires that occur within  
 399 40 samples on these wires. This value was determined  
 400 by examining a simulation of electrons with energies in  
 401 the range of interest. If a cluster spans an unresponsive  
 402 wire, each section was considered as a separate cluster. A  
 403 total number of 553, 319 and 4537 plane-matched clus-

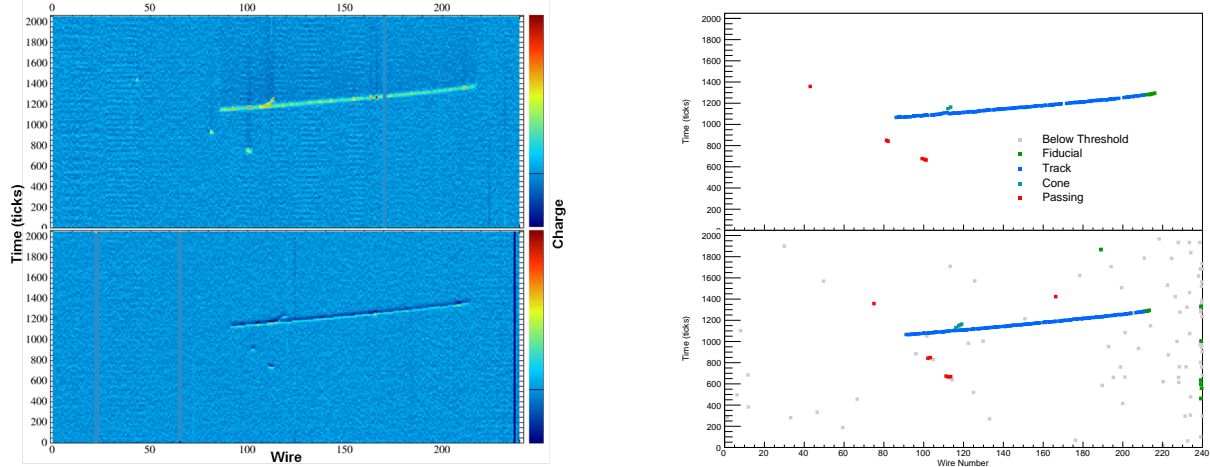


FIG. 4. Left: A raw data neutrino event display with one track reconstructed as a muon and with photon activity (isolated blips). The top image is the collection plane, and the bottom image is the induction plane. Wire number is indicated on the horizontal axis. The vertical axis indicates sample number. Color indicates amount of charge collected. Right: The same event after hit finding and reconstruction. Each square denotes a reconstructed hit. Color indicates whether or not a hit was removed and by which cut (see text). Hits that pass all cuts are in red.

Cut	Percent of Hits Remaining		
	Neutrino	Background	MC
Minimum Peak Height	65%	38%	94%
Maximum Peak Height	58%	37%	84%
Handscanning	54%	29%	78%
Plane Matching	24%	10%	54%

TABLE I. Impact of different cuts for collection plane hits. Cuts are applied sequentially. MC was simulated with no noise.

404 ters were reconstructed, yielding an average of 1.00, 0.16  
 405 and 1.12 clusters per event in the selected neutrino, back-  
 406 ground and MC events, respectively. In neutrino events,  
 407 most of the clusters (75%) are composed of just one hit,  
 408 23% are two hit clusters, and only 2% are clusters with  
 409 more than two hits.

## 410 B. Position Reconstruction

411 We reconstructed the 3D position of a cluster by  
 412 matching the furthest upstream collection plane hit in a  
 413 cluster to the furthest upstream induction plane hit in the  
 414 matched cluster. This yielded a coordinate on the  $yz$ -  
 415 plane. We then included the  $x$ -coordinate of the collec-  
 416 tion plane hit to obtain a 3D position and calculated the  
 417 distance of each cluster with respect to the neutrino inter-  
 418 action vertex. While a cluster may span more than one  
 419 wire in a plane, the distance traveled by the presumed  
 420 Compton-scattered electron creating the cluster is negli-  
 421 gible when compared to the distance from the vertex.

## 422 C. Charge to Energy Conversion

423 To reconstruct the energy associated with each recon-  
 424 structed cluster, first the measured pulse area ( $\text{ADC} \times$   
 425 time) of each hit was converted to charge (number of ion-  
 426 ization electrons) by an electronic calibration factor, then  
 427 a lifetime correction was applied to account for ioniza-  
 428 tion electron loss due to attachment on impurities in the  
 429 liquid argon during drift, as described in [7].

430 Calorimetric reconstruction in a LArTPC requires  
 431 converting the collected charge to the original energy de-  
 432 posited in the ionization process. This requires applying  
 433 a recombination correction which depends on charge de-  
 434 position per unit length  $dQ/dx$  [27]. The low-energy  
 435 photon-induced electrons in the present analysis result in  
 436 just isolated hits or clusters of very few hits, not extended  
 437 tracks, so the effective length of the electron track seen  
 438 by a wire cannot be determined.

439 A different method to estimate the energy from the de-  
 440 posited charge which relies on the assumption that all  
 441 hits passing cuts are due to electrons only has been de-  
 442 veloped. The method uses the NIST table that provides  
 443 the actual track length for electrons in LAr at given en-  
 444 ergies (ESTAR) [31], from 10 keV to 1 GeV. Using this  
 445 table, we can thus approximate the deposited energy den-  
 446 sity  $dE/dx$  by dividing the energy by the track length  
 447 for each row in the table. Using the Modified Box Equa-  
 448 tion [32] to model the recombination effect, we can cal-  
 449 culate the expected  $dQ/dx$  and by multiplying by the  
 450 track length (i.e.  $dx$ ), we obtain the expected amount  
 451 of charge freed from ionization processes by an electron  
 452 at a given energy, as shown in Fig. 5 (left). By using  
 453 the result of a fit, also shown in the Figure, we can now



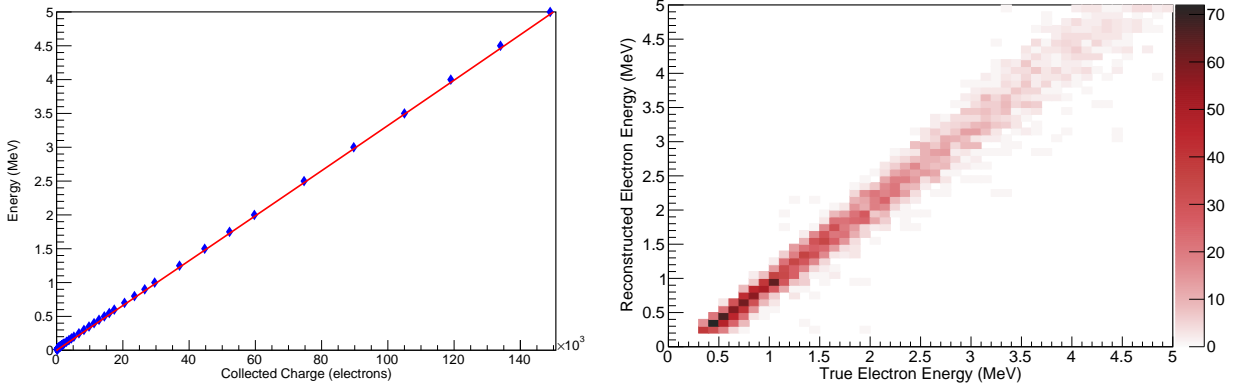


FIG. 5. Left: Energy deposited vs collected charge. Red curve indicates fit used to perform energy calculations from collected charge. Right: Reconstructed energy vs true electron energy using the charge method for a sample of simulated electrons with energies between 0 and 5 MeV. Events where the electron was not detectable are excluded.

454 convert collected charge from the individual hit to de-  
 455 posited energy. The total energy in a cluster is the sum  
 456 of the deposited energy reconstructed for each individ-  
 457 ual hit forming the cluster. To test the efficacy of this  
 458 method, we applied it to a sample of GEANT4 simulated  
 459 electrons propagating in LAr in the energy range of inter-  
 460 est. Figure 5 (right) indicates that it works well. We find  
 461 an detection efficiency of 50% and energy resolution of  
 462 24% at 0.5 MeV, and an efficiency of almost 100% and  
 463 energy resolution of 14% at 0.8 MeV.

#### 464 D. Systematic Uncertainties

465 There are three primary sources of systematic uncer-  
 466 tainty associated with hit and energy reconstruction in  
 467 this analysis. As the electron lifetime varies between  
 468 runs, we expect a variation and uncertainty in the num-  
 469 ber of near-threshold hits that are selected as signal. De-  
 470 spite having precise measurements of electron lifetime  
 471 for all runs, we conservatively account for electron life-  
 472 time uncertainties by re-running FLUKA signal hit selec-  
 473 tions with a 25% increase in either high- or low-lifetime  
 474 runs; the resultant spread in reconstructed multiplicities  
 475 and energies is treated as the systematic uncertainty from  
 476 this source. A second systematic uncertainty arises from  
 477 the choice of a true underlying functional form for the re-  
 478 combination correction. To account for this uncertainty,  
 479 we consider reconstruction of simulated events using the  
 480 unmodified Box Model as described in [32]; deviation  
 481 from the default selection is treated as an uncertainty  
 482 contribution from this source. Finally, there is a 3% error  
 483 associated with the utilized calorimetric calibration con-  
 484 stants, which are fully correlated between all runs. Any  
 485 multiplicity or energy variation arising from a  $\pm 3\%$  shift  
 486 in thresholds and reconstructed energies is treated as an  
 487 uncertainty from this source. Systematic uncertainties in  
 488 reconstructed positions are expected to be small and were

489 not considered in this analysis.

## 490 VI. RESULTS

### 491 A. Comparison of Neutrino and Background Datasets

492 Table II shows distributions for neutrino and back-  
 493 ground datasets. Comparing the distributions leads to the  
 494 conclusion that we have observed a statistically sig-  
 495 nificant sample of neutrino-induced MeV-scale photons.  
 496 Hit and cluster multiplicities are found to be significantly  
 497 higher in the neutrino dataset than in the background  
 498 dataset, with  $1.30 \pm 0.05$  and  $0.21 \pm 0.01$  hits per event,  
 499 respectively. This difference corresponds to an  $21\sigma$  sta-  
 500 tistical excess of signal in the neutrino dataset, which can  
 501 be interpreted as first observation of neutrino-induced  
 502 MeV-scale energy depositions in a LArTPC.

503 This higher neutrino dataset multiplicity is also ac-  
 504 companied by a larger per-event signal occupancy ( $54 \pm$   
 505  $3\%$  in neutrino events versus  $12 \pm 0.8\%$  in background  
 506 events) and total signal hit energy per event (1.1 MeV in  
 507 neutrino events versus 0.19 MeV in background events).

### 508 B. Comparison to MC Simulations

509 A comparison of reconstructed per-event signal multi-  
 510 plicity and total signal energy for data and FLUKA MC  
 511 simulation are shown in Figs. 6 and 7, respectively. MC  
 512 is scaled to the number of events in data.

513 In both data and MC, around half of the events have  
 514 no signal clusters, as expected based on the small Ar-  
 515 goNeuT detector size and the previously-mentioned siz-  
 516 able number of predicted product nuclei in the ground-  
 517 state. Overall, there is good agreement between data and  
 518 FLUKA MC predictions. We find a  $\chi^2/\text{ndf}$  of 7.81/12

Metric	Neutrino Data	Background
Number of hits per event	1.30	0.21
Number of clusters per event	1.00	0.16
Average total signal energy in an event (MeV)	1.11	0.19
Percent of events with at least one signal hit	54%	12%
Average cluster distance from vertex (cm)	22.4	—

TABLE II. Comparison of neutrino and background datasets when examining hits passing all cuts. The difference in the first four metrics indicates neutrino-induced MeV-scale activity is visible.

Metric	De-excitation	Neutron	Total
Number of hits per event	0.48	0.98	1.46
Number of clusters per event	0.35	0.77	1.12
Average event energy (MeV)	0.41	0.76	1.17
Average cluster energy (MeV)	1.18	0.98	1.04
Average hit energy (MeV)	0.86	0.77	0.80
Average cluster distance from vertex (cm)	15.7	23.4	21.0

TABLE III. Relative contributions of de-excitation and neutron-produced photon components in FLUKA MC.

519 (p-value 0.80) for the total reconstructed energy distributions, and a  $\chi^2/\text{ndf} = 12.6/6$  (p-value 0.05) for the cluster multiplicity distribution. Thus, we observe that FLUKA, which incorporates low-level nuclear processes that result in the production of MeV-scale energy depositions following interactions of GeV-scale neutrinos in liquid argon, agrees well with the data. We observe that the largest contributor to the  $\chi^2$  between the data and MC multiplicity distributions is the difference in high-multiplicity events. The modest excess in MC, which spreads over multiple reconstructed energy bins, could be indicative of flaws in the hit selection process, or of imperfections in models or libraries utilized by FLUKA. This feature can be better examined in future high-statistics studies in larger LArTPCs. Finally, we notice a dip in the first bin in Fig. 7, due to detector thresholding, which can vary in data from event to event due to different electron lifetime values.

537 Both components, de-excitation photons and photons produced by interactions of final-state neutrons on argon, are needed to have data-MC agreement. If de-excitation photons are removed from FLUKA distributions, we obtain a  $\chi^2/\text{ndf} = 82.6/12$  for reconstructed energy and  $\chi^2/\text{ndf} = 93.8/6$  for the cluster multiplicity. If neutron-produced photons are removed, we obtain  $\chi^2/\text{ndf} = 194/12$  and  $\chi^2/\text{ndf} = 197/6$  for these same distributions, respectively. To confirm this, we also

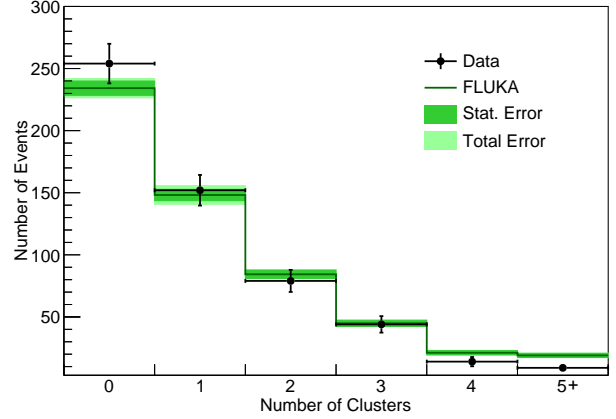


FIG. 6. Cluster multiplicity for neutrino data and FLUKA events. Data points include statistical error. Dark green line indicates FLUKA prediction with background added. Dark green shaded area is statistical error in FLUKA, overlaid on total error (statistical + systematic) for FLUKA in light green shading. MC is normalized to the number of neutrino data events.

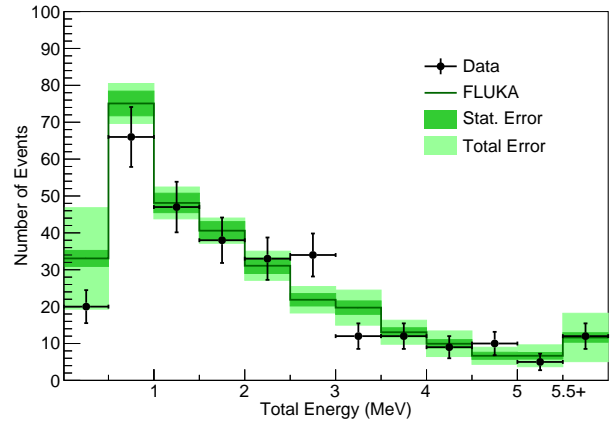


FIG. 7. Total reconstructed energy of MeV-scale energy depositions in an event for neutrino data and FLUKA MC events. Events with no reconstructed energy are not included. Data points include statistical error. Dark green line indicates FLUKA prediction with background added. Dark green shaded area is statistical error in FLUKA, overlaid on total error (statistical + systematic) for FLUKA in light green shading. MC is normalized to the number of neutrino data events.

546 compared ArgoNeuT data with a GENIE MC simulation [33]; existing user interfaces allowed for easy generation of GENIE final states within the LArSoft framework. The same event selection and reconstruction procedure as in FLUKA was applied to GENIE events. As an example, a comparison of reconstructed multiplicity is shown in Fig. 8. The  $\chi^2/\text{ndf}$  is 57.9/6. This disagreement is attributed to the lack of de-excitation photons in the GENIE simulation of neutrino-argon interactions.

554 These results indicate that the observed MeV-scale signals in ArgoNeuT contain both de-excitation and



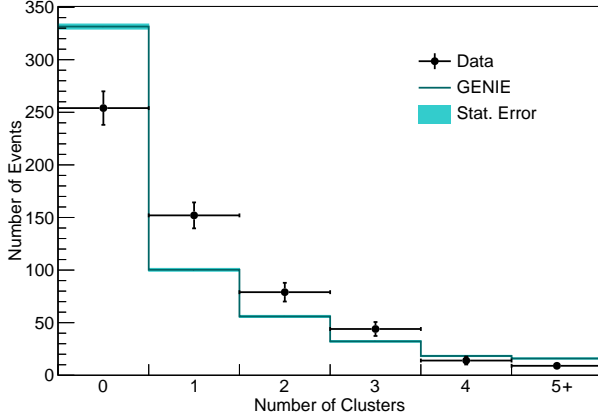


FIG. 8. Distribution of cluster multiplicity for neutrino data and GENIE events. Data points include statistical error. Dark blue indicates GENIE prediction (no de-excitation photons). Light blue shaded area indicates statistical error for GENIE prediction. MC is normalized to the number of neutrino data events.

neutron-produced photons. The contribution of each of these sources to the total activity in an event as given by the FLUKA simulation is shown in Table III. We find that we cannot distinguish between the two sources of photons by examining the energy of a hit or cluster alone, but we do see a difference in the distance of a cluster with respect to the neutrino interaction vertex. The distribution of these distances is seen in Fig. 9. Photons produced by de-excitation of the final-state nucleus tend to be concentrated at low distances, while photons produced by inelastic neutron scattering dominate at high distances.

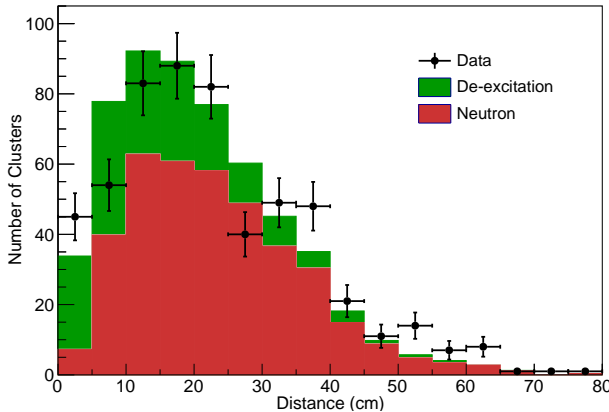


FIG. 9. Distributions of cluster position with respect to the neutrino interaction vertex in neutrino data and FLUKA events. Data includes statistical error. Green indicates contribution of photons from de-excitation of the final-state nucleus. Red indicates contribution of photons from inelastic neutron scattering. MC is area normalized to data.

## VII. CONCLUSION

The ability to reconstruct activity at the MeV scale in a LArTPC is crucial for future studies of supernova, solar, and beam neutrino interactions. In addition, studies of low scale new physics scenarios, for example millicharged particles, light mediators, and inelastic scatterings with small splittings (see e.g. Refs. [34–36]), could invaluably profit from such low energy reconstruction. By studying low-energy depositions produced by photons in ArgoNeuT neutrino interactions and comparing to simulation, we have shown that such a reconstruction is possible. Performing this study required the creation of new techniques for low-energy LArTPC reconstruction. By reconstructing photons produced by nuclear de-excitation and inelastic neutron scattering, we have extended the LArTPC’s range of physics sensitivity down to the sub-MeV level, reaching a threshold of 0.3 MeV in this analysis. This range now spans more than three orders of magnitude, up to the GeV level.

In our study of low-energy depositions in ArgoNeuT neutrino events, we found 553 clusters with an average of  $1.30 \pm 0.05$  hits per event and an average energy of  $1.11 \pm 0.16$  MeV per event. Signal cluster multiplicities in neutrino events outnumbered those in nearby background events, establishing a clear neutrino-based origin for these MeV-scale features. These and other cluster properties matched those predicted for photons due to inelastic neutron scattering and de-excitation of the final-state nucleus in FLUKA using its model of nuclear physics processes at the MeV-scale. Removal of either of these event classes significantly worsens the level of data-simulation agreement.

This analysis represents the first-ever reported detection of de-excitation photons or final-state neutrons produced by beam neutrino interactions in argon. Both of these particle classes could provide valuable new avenues of investigation for physics reconstruction in LArTPCs. Reconstruction of MeV-scale neutron-produced features may enable some level of direct reconstruction of final-state neutron energies or multiplicities, which would provide a valuable new handle on one of the dominant expected differences between neutrino and antineutrino interactions in liquid argon. Precise reconstruction of de-excitation photon multiplicities and energies will improve overall reconstruction of neutrino energies, particularly for those at lower energies, such as supernova and solar neutrinos. Future MC studies and higher-statistics datasets from future large LArTPCs will provide additional understanding of the value of these newly-detected MeV-scale features.

## VIII. ACKNOWLEDGEMENTS

This manuscript has been authored by Fermi Research Alliance, LLC under Contract No. DE-AC02-07CH11359 with the U.S. Department of Energy, Office of Science, Office of High Energy Physics. We gratefully acknowledge the cooperation of the MINOS Collaboration in providing their data for use in this analysis. We wish to acknowledge the support of Fermilab, the Department of Energy, and the National Science Foundation in ArgoNeuT's construction, operation, and data analysis. We also wish to acknowledge the support of

the Neutrino Physics Center (NPC) Scholar program at Fermilab, ARCS Foundation, Inc and The Royal Society (United Kingdom).

This material is based upon work supported by the U.S. Department of Energy, Office of Science, Office of Workforce Development for Teachers and Scientists, Office of Science Graduate Student Research (SCGSR) program. The SCGSR program is administered by the Oak Ridge Institute for Science and Education (ORISE) for the DOE. ORISE is managed by ORAU under contract number DE-SC0014664.

- 
- [1] R. Acciarri *et al.* (ArgoNeuT), Phys. Rev. Lett. **108**, 161802 (2012).
- [2] R. Acciarri *et al.* (ArgoNeuT), Phys. Rev. **D89**, 112003 (2014).
- [3] R. Acciarri *et al.* (ArgoNeuT), Phys. Rev. **D90**, 012008 (2014).
- [4] R. Acciarri *et al.* (ArgoNeuT), Phys. Rev. Lett. **113**, 261801 (2014), [erratum: Phys. Rev. Lett. **114**, no. 3, 039901 (2015)].
- [5] O. Palamara (ArgoNeuT), JPS Conf. Proc. **12**, 010017 (2016).
- [6] R. Acciarri *et al.* (ArgoNeuT), Phys. Rev. **D96**, 012006 (2017).
- [7] R. Acciarri *et al.* (ArgoNeuT), (2018), arXiv:1804.10294 [hep-ex].
- [8] C. Adams *et al.* (MicroBooNE), (2018), arXiv:1805.06887 [hep-ex].
- [9] M. Antonello *et al.* (ICARUS), Eur.Phys.J. **C73**, 2345 (2013).
- [10] F. Cavanna, M. Kordosky, J. Raaf, and B. Rebel (LAR-IAT), (2014), arXiv:1406.5560 [physics.ins-det].
- [11] R. Acciarri *et al.* (MicroBooNE), JINST **12**, P02017 (2017).
- [12] M. Antonello *et al.* (LAR1-ND, ICARUS-WA104, MicroBooNE), (2015), arXiv:1503.01520 [physics.ins-det].
- [13] C. Adams *et al.* (LBNE), (2013), arXiv:1307.7335 [hep-ex].
- [14] B. Abi *et al.* (DUNE), (2017), arXiv:1706.07081 [physics.ins-det].
- [15] R. Acciarri *et al.* (MicroBooNE), JINST **12**, P09014 (2017).
- [16] S. Amoroso *et al.* (ICARUS), Eur. Phys. J. **C33**, 233 (2004).
- [17] W. Foreman (LAR-IAT), JINST **11**, C01037 (2016).
- [18] K. Scholberg, *Neutrino physics and astrophysics. Proceedings, 19th International Conference, Neutrino 2000, Sudbury, Canada, June 16-21, 2000*, Nucl. Phys. Proc. Suppl. **91**, 331 (2001), [331(2000)].
- [19] C. Grant and B. Littlejohn, *Proceedings, 38th International Conference on High Energy Physics (ICHEP 2016): Chicago, IL, USA, August 3-10, 2016*, PoS **ICHEP2016**, 483 (2016).
- [20] H. Berns *et al.* (CAPTAIN) (2013) arXiv:1309.1740 [physics.ins-det].
- [21] J. Spitz, Phys. Rev. D **85**, 093020 (2012).
- [22] D. Akimov *et al.* (CSI), in *Proceedings, 2013 Community Summer Study on the Future of U.S. Particle Physics: Snowmass on the Mississippi (CSS2013): Minneapolis, MN, USA, July 29-August 6, 2013* (2013) arXiv:1310.0125 [hep-ex].
- [23] S. J. Brice *et al.*, Phys. Rev. **D89**, 072004 (2014).
- [24] A. Ferrari, P. R. Sala, A. Fasso, and J. Ranft, *FLUKA: A multi-particle transport code (Program version 2005)*, Tech. Rep. (2005).
- [25] G. Battistoni *et al.*, Annals of Nuclear Energy **82**, 10 (2015).
- [26] G. Battistoni, A. Ferrari, M. Lantz, P. R. Sala, and G. I. Smirnov, in *CERN-Proceedings-2010-001* (2010) pp. 387–394, proceedings of 12th International Conference on Nuclear Reaction Mechanisms, Varenna, Italy, 15-19 June 2009.
- [27] C. Anderson *et al.* (ArgoNeuT), JINST **7**, P10019 (2012).
- [28] D. G. Michael *et al.* (MINOS), Nucl. Instrum. Meth. **A596**, 190 (2008).
- [29] National Nuclear Data Center, information extracted from the Chart of Nuclides database, <http://www.nndc.bnl.gov/chart/>.
- [30] E. L. Snider and G. Petrillo, *Proceedings, 22nd International Conference on Computing in High Energy and Nuclear Physics (CHEP2016): San Francisco, CA, October 14-16, 2016*, J. Phys. Conf. Ser. **898**, 042057 (2017).
- [31] Berger, M.J., Coursey, J.S., Zucker, M.A., and Chang, J. (2005), ESTAR, PSTAR, and ASTAR: Computer Programs for Calculating Stopping-Power and Range Tables for Electrons, Protons, and Helium Ions (version 1.2.3). [Online] Available: <http://physics.nist.gov/Star> [2017, December 8]. National Institute of Standards and Technology, Gaithersburg, MD.
- [32] R. Acciarri *et al.* (ArgoNeuT), JINST **8**, P08005 (2013).
- [33] C. Andreopoulos *et al.*, Nucl. Instrum. Meth. **A614**, 87 (2010).
- [34] S. N. Gninenko, Phys. Lett. **B710**, 86 (2012), arXiv:1201.5194 [hep-ph].
- [35] G. Magill, R. Plestid, M. Pospelov, and Y.-D. Tsai, (2018), arXiv:1806.03310 [hep-ph].
- [36] E. Bertuzzo, S. Jana, P. A. N. Machado, and R. Zukanovich Funchal, (2018), arXiv:1808.02500 [hep-ph].